

# Effect of Nb cationic substitution on Raman spectra of $\text{SrBi}_2\text{Ta}_2\text{O}_9$ thin films

O. M. Fesenko<sup>1</sup>, A. D. Yaremkevich<sup>1</sup>, T. V. Tsebrienko<sup>1</sup>, O. P. Bydnyk, A. V. Semchenko<sup>2</sup>, V. V. Sidski<sup>2</sup>, and A. N. Morozovska<sup>1\*</sup>

<sup>1</sup>*Institute of Physics, National Academy of Sciences of Ukraine, 46, pr. Nauky, 03028 Kyiv, Ukraine*

<sup>2</sup>*Francisk Skorina Gomel State University, Belarus, 246019, Gomel, 104, Sovetskaya str.*

## ABSTRACT

In the present work micro-Raman spectroscopy has been used to understand the lattice dynamics of cation substituted  $\text{SrBi}_2\text{Ta}_2\text{O}_9$  (SBT) thin films. Different concentrations of Nb were introduced into SBT lattices. Incorporation of Nb ion at Ta-site was confirmed by decrease in the lattice parameters calculated from x-ray diffraction data. Substitution of Nb at Ta-site of SBT did not influence the low frequency Raman modes of SBTN. However, it showed a pronounced influence on the O-Ta-O stretching modes by shifting and splitting the mode frequency at  $810\text{ cm}^{-1}$ . The relative intensity of (200) peak in x-ray diffraction increased with the increase of the Nb concentration. Landau approach was used to explain the experimentally observed fraction of perovskite phase in SBTN allowing possible appearance of finite size effects related with nanogranular structure of the studied SBTN films.

## 1. INTRODUCTION

Ferroelectric materials, such as, layered ferroelectric perovskites strontium bismuth tantalate  $\text{SrBi}_2\text{Ta}_2\text{O}_9$  (SBT) and niobate  $\text{SrBi}_2\text{Nb}_2\text{O}_9$  (SBN) have high dielectric permittivity, high piezoelectric and pyroelectric coefficients, optimal electro-optic properties, and robust polarization switching [1, 2, 3]. These materials, due to their intriguing electronic, ferroelectric and electrophysical properties have been recognized as a prominent candidate for applications in non-volatile ferroelectric memories (NvFRAM) [4, 5, 6, 7] because of negligible fatigue, low leakage currents, and ability to maintain ferroelectricity in the form of thin films [8, 9, 10].

---

\* corresponding author, e-mail: [anna.n.morozovska@gmail.com](mailto:anna.n.morozovska@gmail.com)

Recently SBT ferroelectric thin films have been extensively investigated for nonvolatile random access memory applications due to their excellent ferroelectric properties on Pt electrodes. It's well known that the high post annealing temperature required and low remanent polarization are the two major barriers, which hinder the full commercial. In order to eliminate these two problems, several groups have attempted different methods such as forming the solid solutions of  $\text{SrBi}_2(\text{Ta}_x\text{Nb}_{1-x})_2\text{O}_9$  (SBTN) [11, 12] changing the stoichiometry of SBT, and controlling the oxygen pressure during the annealing process [13, 14]. Also, it needs take into account that in the case of undoped SBT, it is still a challenge to obtain large remanent polarization at low annealing temperatures [15]. As for majority of perovskites, intrinsic defects, chemical doping, grain orientation, post sintering and annealing strongly influence their microstructural, dielectric, piezoelectric, pyroelectric, ferroelectric and other electrophysical properties [16].

In this work, we report on the optical and structure characterization of SBT thin films doped by Nb in concentration ( $x=10, 20, 30, 40$  and  $50\%$ ) and modified by annealing method under  $700$ ,  $800$  and  $900\text{ }^{\circ}\text{C}$ . Here we report the micro-Raman scattering study of thin film SBTN prepared by the sol-gel method. Other experimental techniques were also employed in order to characterize the films. Landau approach is used to explain the experimentally observed fraction of perovskite phase in SBTN allowing possible appearance of finite size effects related with nanogranular structure of the studied SBTN films.

## 2. EXPERIMENTAL DETAILS

The SBT material belongs to the  $\text{ABi}_2\text{B}_2\text{O}_9$  perovskite-like and has a face-centered orthorhombic unit cell, consisting of  $\text{TaO}_6$  octahedrons (see **Fig. 1**). The spontaneous polarization vector lies in the plane of these layers. The material has high temperature phase transition ( $T_c$ ) around  $335\text{ }^{\circ}\text{C}$  [17].

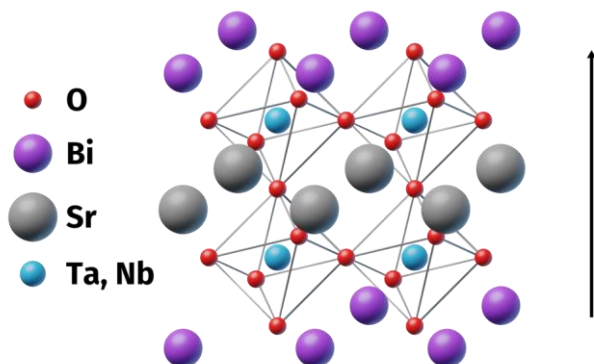
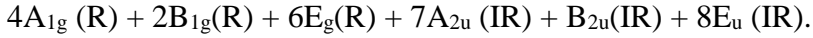


**Fig. 1.** SBTN structure

As a first approximation, it is helpful to assign tetragonal symmetry to the  $\text{SrBi}_2\text{Ta}_2\text{O}_9$  material above the Curie temperature. It corresponds to a  $\text{I}_{4/\text{mmm}}$  space group. In this symmetry the following Raman and IR modes should be active [18]:



Below the Curie temperature ( $T < T_c$ ), an orthorhombic symmetry is expected in SBT, so that each  $\text{E}_g$  mode is split in  $\text{B}_{2g} + \text{B}_{3g}$ . A splitting at room temperature in two components must be consistent with the orthorhombic distortion [19, 20].

SBT has an orthorhombic crystal structure with the  $\text{A}21\text{am}$  space group in the ferroelectric phase, which becomes tetragonal at  $T$  above  $335^\circ\text{C}$  with the  $\text{I}4 / \text{mmm}$  space group in the paraelectric phase. The inclusion of any cations with Sr, Bi or Ta substitution involves a change in crystal structure and symmetry depending on the valence and ionic radii of the cations. Nb has smaller ionic radii than Ta, and its placement at the Ta-location of SBT will change the bond length of ions inside the layered unit cell of SBT. Given the mass of Nb and Ta, it is expected that a smaller mass of Nb can shift the vibrational modes to higher frequencies. Because the mass of Nb is less than Ta, the effective mass of the unit cell will also be smaller and smaller after the introduction of more Nb.

## 2.1. Materials and methods

The starting product for sol preparation and subsequent formation of the capacitor  $\text{SrBi}_2(\text{Ta}_x\text{Nb}_{1-x})_2\text{O}_9$  layer was 0/01 mol/l solution of inorganic metal salts (tantalum, niobium and rare earth chlorides, bismuth and strontium nitrates in toluene). Deposition of SBTN films on substrate was performed by spin-coating of stable solution at the substrate rotation frequency from 800 to 1500 rot/min during 2 to 5 seconds. Organic solvent was removed by multi-stage drying under temperature increase from 80 to 350 for 6 min. Required thickness of SBT and SBTN films (200-300 nm) was obtained by layer-by-layer deposition of 2-3 sol-gel layers with heat treatment of each layer at temperature of  $700\text{ }^\circ\text{C}$ . Perovskite SBTN structure was formed during annealing at  $(700\text{-}900)\text{ }^\circ\text{C}$  for 30 min.

The crystallographic orientation of the films was analyzed by x-ray diffraction (XRD) in the glancing-angle detector scan mode. Raman spectra have been measured using a InVia micro-Raman spectrometer (Renishaw) equipped with a confocal DM2500 Leica optical microscope, a thermoelectrically cooled CCD as a detector and a laser operating at a wavelength  $\lambda = 633\text{ nm}$

excitation from the He–Ne laser. Spectra of IR light absorption were measured with FT-IR spectrometer Vertex 70 with microscope Hyperion 1000 from Bruker Optics.

### 3. EXPERIMENTAL RESULTS AND DISCUSSION

From the structure point of view, SBT belongs to the bismuth layered perovskite family with the lattice parameter of  $a=b=50.552$  nm and  $c=2.502$  nm in terms of orthorhombic structure. The highly anisotropic structure of SBT results in the ferroelectric properties to be strongly dependent on the crystallographic orientation of the film. It has been reported that the ferroelectric properties of SBT thin films in the  $a - b$  plane are much better than those along the  $c$  axis [21]. This is because the continuous perovskite structure only exists in the  $a - b$  plane. Therefore, preparation of SBT thin films with (200) preferential orientation is highly desirable. **Figure 2** shows the XRD patterns of SBTN thin films doped by Nb (x=10, 20, 30, 40 and 50%). As the concentration Nb increased, the peak intensity of the films increased, indicating grain growth. In addition, the intensity of (200) peak increased for film SBTN doped by Nb at the concentration 10% and 30%. These results suggest that the structure of SBT thin films can be controlled by the Nb-doped process. The films showed a polycrystalline nature with a (115) orientation, which is preferable for ferroelectric properties.

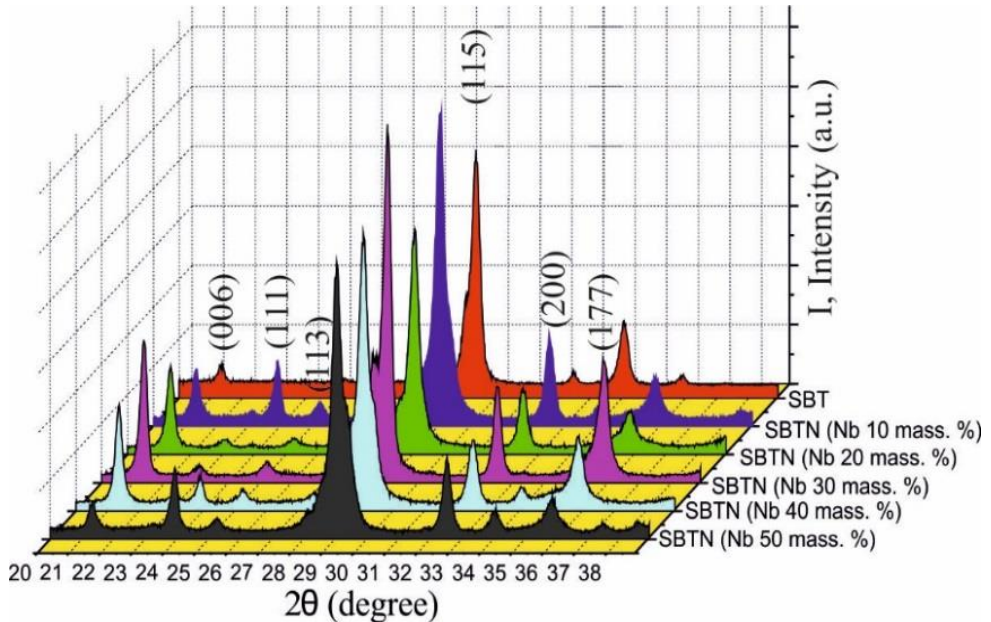


**Fig. 2.** XRD patterns of SBTN films with various Nb contents [22].

We measured Raman spectra of thin  $\text{SrBi}_2\text{Ta}_2\text{O}_9$  films annealed at different temperatures and doped with different percent of substituting Nb atoms (from 10 to 50%). In general, the Raman results indicate that the SBTN films are polycrystalline. The sintering temperature-dependent Raman spectra of the SBT ceramics are presented in **Fig. 3**.

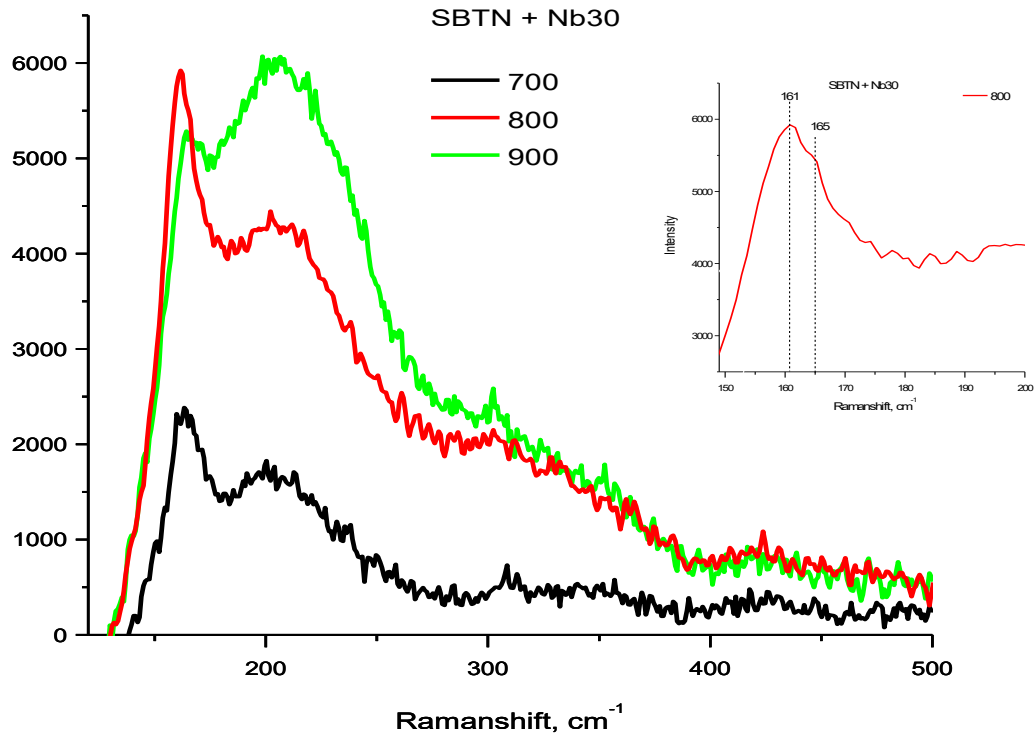


**Fig. 3.** The sintering temperature-dependent Raman spectra of the SBT ceramics under 700, 800 and 900 °C

Other studies have reported that the Raman spectrum of a SBT ceramics exhibit intense peaks at approximately 163, 210, 600, and 805 cm<sup>-1</sup> and that the other peaks at 319, 356, and 455 cm<sup>-1</sup> corresponded to weak features [23, 24]. Our result was in agreement with these characteristic bands as bands at approximately 161, 208, 319, 356, 450, 590, and 810 cm<sup>-1</sup> were prominent in the SBT ceramics in this study. The band at 161 cm<sup>-1</sup> is associated with the lattice vibration of the Ta+ 5 ions along the z direction (TO mode A1g) [25]. With increasing temperature from 700 to 800 °C, the band at 161 cm<sup>-1</sup> shifted to 162 cm<sup>-1</sup> and shoulder appears at 165.7 cm<sup>-1</sup> (Fig. 3). With increasing temperature from 800 to 900 °C, the shoulder at 161 cm<sup>-1</sup> disappears and the main band is located near 165 cm<sup>-1</sup>.

As one can see from Fig. 4, the granular structure of the film increases with increasing the temperature from 700 to 800 °C and 900°C. This is believed to be due to the grain growth and higher density of the films by increasing the annealing temperature. The increased temperature from 700 to 800°C led to improved crystallinity. It can be assumed that the grain growth and the preferential orientation to the a – b plane, as was observed in XRD patterns (see Fig. 2).

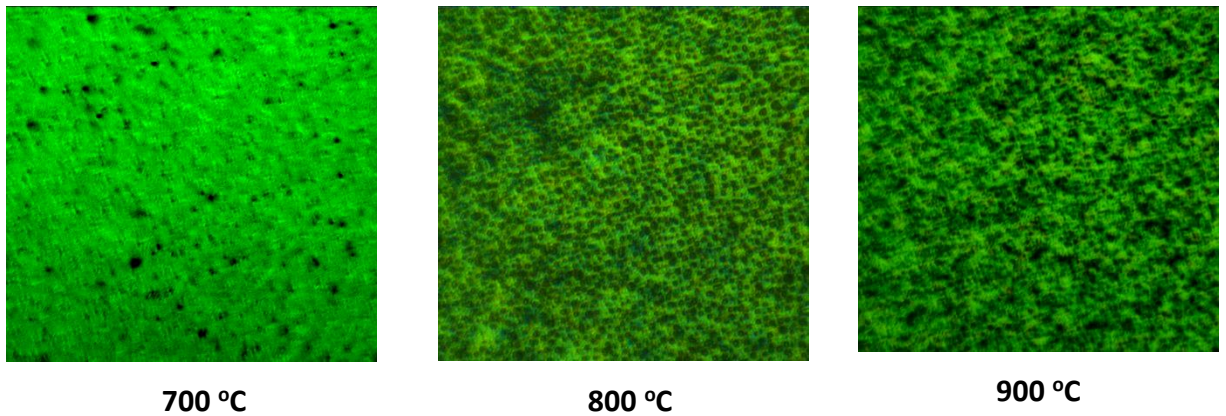


**Fig. 4.** Microscopic image of thin SrBi<sub>2</sub>Ta<sub>2</sub>O<sub>9</sub> films doped Nb with 30%

The A<sub>1g</sub> mode shifts to higher/lower wave number is relation to the grain growth, therefore, the grain size [faster growth of the (00l) planes] of the SBT ceramic increases, and it will be leading to the A<sub>1g</sub> mode shifts to higher wave numbers, as shown in **Figs. 5**. The nondegenerate A<sub>1g</sub> mode, vibrate in the plane perpendicular to the c axis, and the shift occurs because the Ta+ 5 ions are replaced by the lower mass Nb ions. In addition, it known that the A<sub>1g</sub> mode behavior is responsible for the phase transition in SBT sample.

In terms of the Raman analysis, it can be observed that the band around  $\sim 820 \text{ cm}^{-1}$  is sensitive to the SBTN crystallization degree. The frequency of this band, in the SBTN films, changes from 810 to 830  $\text{cm}^{-1}$ . These frequency variations seem to be associated not only with Nb-doped concentration, but also with the amount of defects (atoms in non-equilibrium positions, impurities, incomplete solid state reaction, etc.) present in the film. This prominent feature corresponds to the A<sub>1g</sub> mode, and is associated with the symmetric stretching of the TaO<sub>6</sub>, octahedron [13]. The Raman band around 163  $\text{cm}^{-1}$  is assigned to the A<sub>1g</sub>, mode. The sharp and intense Raman band at 60  $\text{cm}^{-1}$  corresponds to the rigid-layer mode also found in familiar systems [11]. The bands in the range 200-300  $\text{cm}^{-1}$  can be due to O-Ta-O bending modes, which are likely to be of B<sub>2g</sub>+B<sub>3g</sub> origin due to the degeneracy lifting of E<sub>g</sub> species. The band around 600  $\text{cm}^{-1}$  can be assigned to a Ta-O-Ta motion. These bonds, which share their oxygen atom with another Ta atom.

The peaks at approximately 600 and 810  $\text{cm}^{-1}$  are attributed to the internal vibration of the TaO<sub>6</sub> octahedron (see the **Fig. 5**). However, the oxygen ions contributing to the two bands are different. The band at 600  $\text{cm}^{-1}$  can be attributed to the vibration of the oxygen ion (O<sub>2</sub>) at the apex of the TaO<sub>6</sub> octahedron. Moreover, the band at 810  $\text{cm}^{-1}$  can be attributed to the vibration of oxygen ions (O<sub>4</sub>, O<sub>5</sub>) in the TaO<sub>6</sub> octahedron (**Fig. 5**). For better understanding about this mode, the de-convolution of SBT ceramic Raman spectra at 810  $\text{cm}^{-1}$  band by using the Gaussian was fit for films under 700, 800 and 900°C. It was found that the band at 810  $\text{cm}^{-1}$  for SBT films under

different temperatures decomposes into one single peak, which is corresponding to  $\text{TaO}_6$  mode. For example, in **Fig. 6** you can see the de-convolutions Raman band at  $810 \text{ cm}^{-1}$  under  $800 \text{ }^\circ\text{C}$  for SBT ceramic with and without doping with Nb. As sintering temperature was  $800 \text{ }^\circ\text{C}$ , the peaks at  $810 \text{ cm}^{-1}$  and  $826.7 \text{ cm}^{-1}$  were corresponding to  $\text{TaO}_6$  mode and B-site substitution modes, respectively.

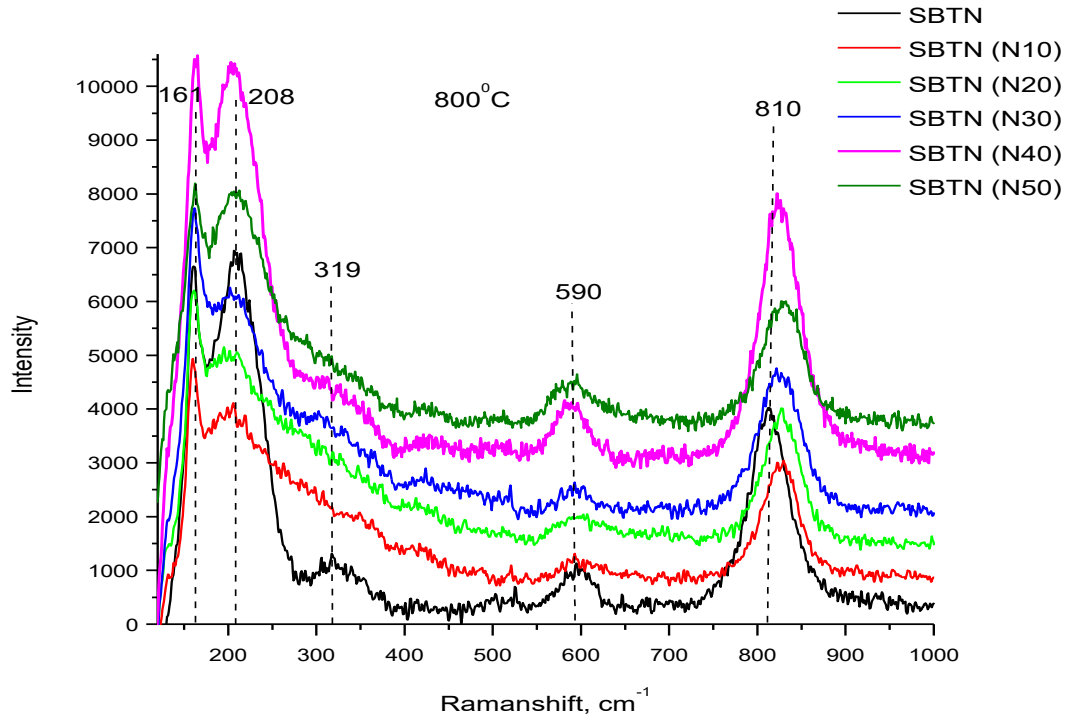


**Fig. 5.** Raman spectra of  $\text{SrBi}_2(\text{Ta}_x\text{Nb}_{1-x})_2\text{O}_9$  films doped with different percentages of Nb substitution atoms ( $x = \text{from } 10 \text{ to } 50\%$ ) at annealing  $T=800^\circ\text{C}$ .

The ratio of peaks  $161 \text{ cm}^{-1}$  to  $208 \text{ cm}^{-1}$  increases with increasing concentration of Nb substituent atoms from 10 to 30%, which coincides with the results of Ref.[13]. Modes above  $300 \text{ cm}^{-1}$  and  $590 \text{ cm}^{-1}$  correspond to the rigid lattice mode, in which all shifts of negative and positive ions are equal and opposite. In the case of pure SBT, the octahedral mode (also known as the breathing mode) has a frequency of  $810 \text{ cm}^{-1}$  and, when replaced by Nb atoms, expands and shifts to higher wavelengths [11]. A similar shift was observed for all Nb concentrations in the sample.

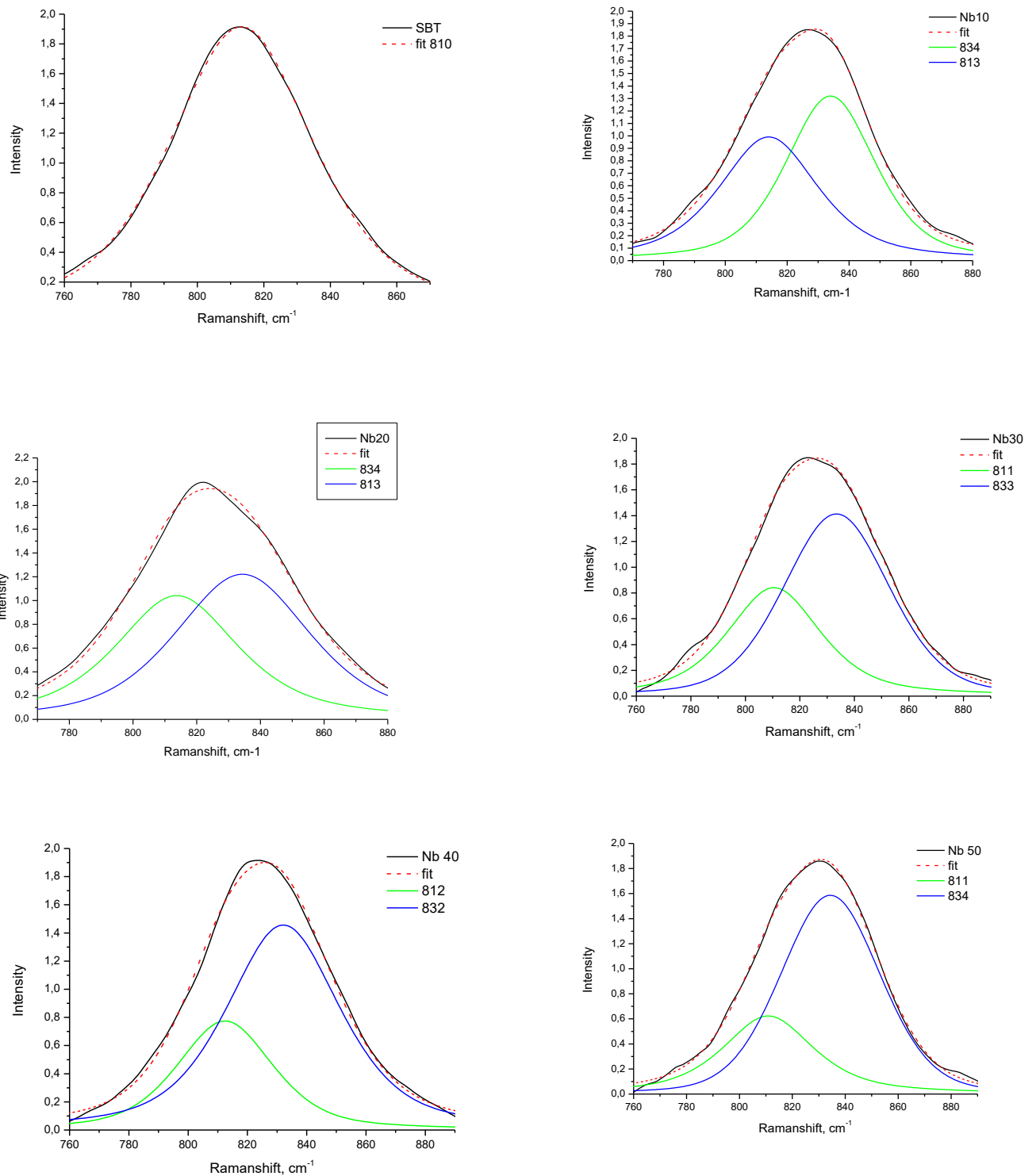


**Fig. 6.** Curve fitting of the band around  $810-830\text{ cm}^{-1}$

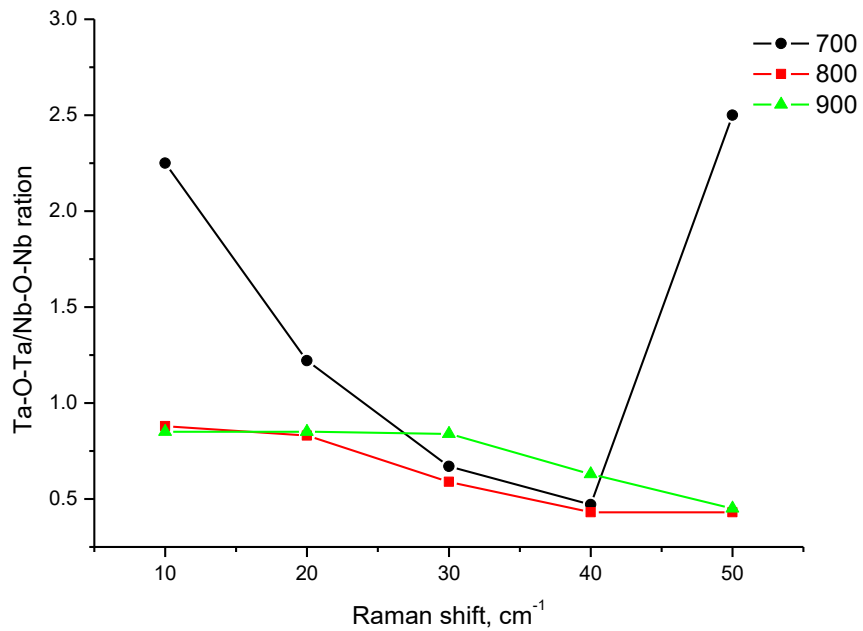


**Fig. 7.** The change in the peak maximum (band 810-840  $\text{cm}^{-1}$ ) depending on the concentration of Nb dopant

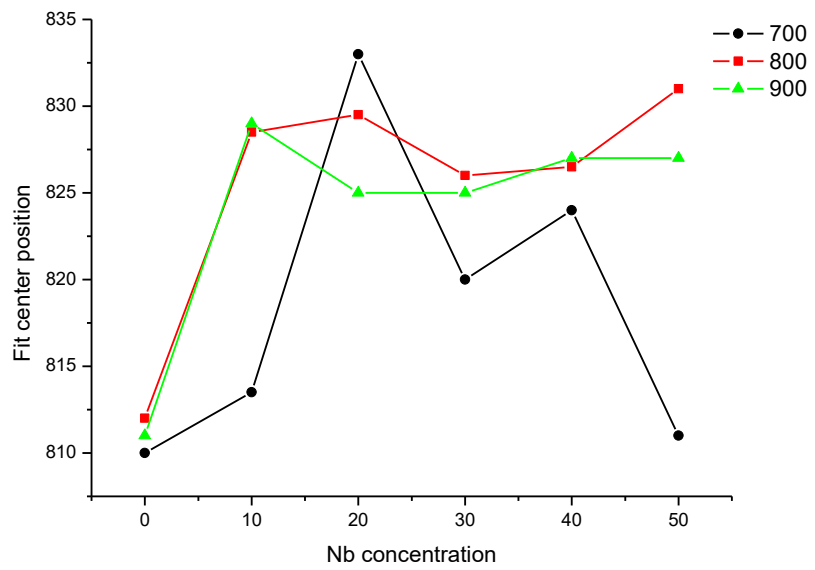


**Fig. 8.** Assignment of the intensity of the fit component of the Raman band at 810  $\text{cm}^{-1}$  to the intensity of the fit component at 840  $\text{cm}^{-1}$

## 4. LANDAU MODEL FOR THE DESCRIPTION OF THE PEROVSKITE PHASE FRACTION IN SBTN

The finite size effect on phase transitions in  $\text{SrBi}_2\text{Ta}_2\text{O}_9$  nanoparticles have been investigated by *in situ* Raman scattering by Yu et al [26], and by thermal analysis and Raman spectroscopy by Ke et al [27]. The finite size and Nb doping effects impact on the phase diagrams, polar and dielectric properties of the SBTN nanogranular films [28, 29]. These effects can be described using the phenomenological Landau approach, taking into account the effect of Nb impurity on the structural ferrodistortion of SBTN and the charge state of this (nominally isovalent) impurity. Thus, the addition of Nb increases the Curie temperature  $T_C$ , and thus improves the ferroelectric properties. Assume that at low concentrations of Nb this dependence decomposes into a series of impurity concentrations  $x$ ,  $T_C(x) = T_C(1 + \sum_{i=1}^n a_i x^i)$ , where  $a_i$  are unknown decomposition coefficients. However, with a further increase in  $x$ , the disorder in the system of oxygen octahedrons increases, because Nb and Ta have different force matrices. The degree of disorder is the maximum for  $x = 50\%$ , and with further increase, we gradually move to the ferroelectric SBN. The effect of variable valence is also not excluded, although it is unlikely to play a key role. The increase in disorder affects the magnitude of spontaneous polarization due to nonlinear interaction with the structural subsystem and the correlation of the order parameter. We assume that the nonlinearity also decomposes into a series of  $x$  (because it is at least an even interaction),  $\beta(x) = \beta_t(1 + \sum_{i=1}^n b_i x^i)$ , where  $b_i$  are unknown decomposition coefficients. In this simplest model we have the following  $x$ -dependent coefficients in the SBTN Landau free energy:

$$F = \frac{\alpha^*(T,x)}{2} P^2 + \frac{\beta(x)}{4} P^4 + \frac{\gamma}{6} P^6 - PE \quad (1)$$

Here  $\mathbf{P}$  is the polarization,  $\mathbf{E}$  is the electric field, and  $\alpha, \beta, \gamma$  are the coefficients of expansion into  $P$ -series. Due to the finite size effect related with the films nanogranular structure, the “effective” coefficient  $\alpha(T,x)$  can depend on the average sizes of the grains, which are modeled by nanoellipsoids with semi-axes  $R$  and  $L$  [29]:

$$\alpha^*(T,x) = \alpha(T,x) + \frac{n_d}{\varepsilon_0[\varepsilon_b n_d + \varepsilon_e(1-n_d) + n_d(D/\lambda)]}, \quad \alpha(T,x) = \alpha_T[T - T_C(x)] \quad (2a)$$

Here  $\varepsilon_b$  and  $\varepsilon_e$  are the dielectric permittivity of ferroelectric background [30] and external media respectively,  $n_d = \frac{1-\xi^2}{\xi^3} \left( \ln \sqrt{\frac{1+\xi}{1-\xi}} - \xi \right)$  is the depolarization factor,  $\xi = \sqrt{1 - (R/L)^2}$  is the eccentricity ratio of ellipsoid with a shorter semi-axes  $R$  and longer semi-axis  $L$  [31]; and  $D$  is the ellipsoid semi-axis ( $R$  or  $L$ ) in the direction of spontaneous polarization  $P$ .

The dielectric stiffness  $\alpha(T, x)$  and the nonlinearity  $\beta(x)$  can be written as follows:

$$\alpha(T, x) = \alpha_t \left( T - T_C (1 + \sum_{i=1}^n a_i x^i) \right), \quad \beta(x) = \beta_t (1 + \sum_{i=1}^n b_i x^i). \quad (2b)$$

Where  $T$  is the absolute temperature,  $T_C$  is the Curie temperature, the coefficients  $\alpha_t$  and  $\beta_t$  are positive. Coefficient  $\gamma \geq 0$ . For the case of phase transitions of the second kind,  $\gamma$  can be neglected, and then the spontaneous polarization and coercive field are equal to:

$$P_S(T, x) = \sqrt{-\frac{\alpha(T, x)}{\beta(x)}}, \quad E_C(T, x) = -\frac{2}{3} \alpha(T, x) \sqrt{\frac{-\alpha(T, x)}{3\beta(x)}}. \quad (3a)$$

Knowing  $P_S(T, x)$  and  $E_C(T, x)$  from the experiment, we can determine the coefficients of Landau expansion  $\alpha(T, x)$  and  $\beta(x)$ :

$$\alpha(T, x) = -\frac{3\sqrt{3}}{2} \frac{E_C(T, x)}{P_S(T, x)}, \quad \beta(x) = -\frac{\alpha(T, x)}{P_S^2(T, x)} \equiv \frac{3\sqrt{3}}{2} \frac{E_C(T, x)}{P_S^3(T, x)}. \quad (3b)$$

Since  $T_C \approx (335 - 378)^\circ\text{C}$  for SBT and  $T_C \approx 115^\circ\text{C}$  for SBN [32], the Curie-Weiss constant  $\alpha_t$  can be determined from the value of the linear dielectric constant of SBT at room temperature, for which the formula  $\frac{1}{2\varepsilon_0\alpha_t(T_C-T)}$  and its value 1280 for a bulk homogeneous sample.

We obtain the value  $\alpha_t = (1,23292 - 1,40122) \cdot 10^5$  m/CF. The dependences of the Landau expansion coefficients  $\alpha(T, x)$  and  $\beta(x)$  on the Nb concentration can be adjusted by means of polynomial functions by fitting the experimental values of spontaneous polarization and coercive field.

The experimental data from **Table 1** were used to fit the experimental results. The results of fitting  $P_S(T, x)$  and  $E_C(T, x)$  using polynomial functions of the 4th order and equations (3a) are shown in **Fig.9a** and **9b**, in accordance. Figures **9c** and **9d** show the dependences of the Landau free energy coefficients  $\alpha(T, x)$  and  $\beta(x)$  on the Nb concentration (as a percentage), calculated from equations (3b) for SBTN at room temperature. As follows from **Fig. 9a**, SBTN films with Nb content of 10 and 20 wt. % have the highest spontaneous polarization [33].

**Table 1.** - Dependence of polar characteristics of SBT and SBTN on Nb content [33].

Parameters	SBT	SBTN (in % Nb)				
		0	10	20	30	40
Content of Nb, mass %	0	10	20	30	40	50
Perovskite phase, %	65	86	85	77	76	70
Spontaneous polarization C/m <sup>2</sup>	0,59	0,79	0,70	0,51	0,58	0,21
Coercive field, kV/m	280	390	370	330	260	100

Bulk dielectric susceptibility at room temperature	1280	NA	NA	NA	NA	NA
NA – no data						

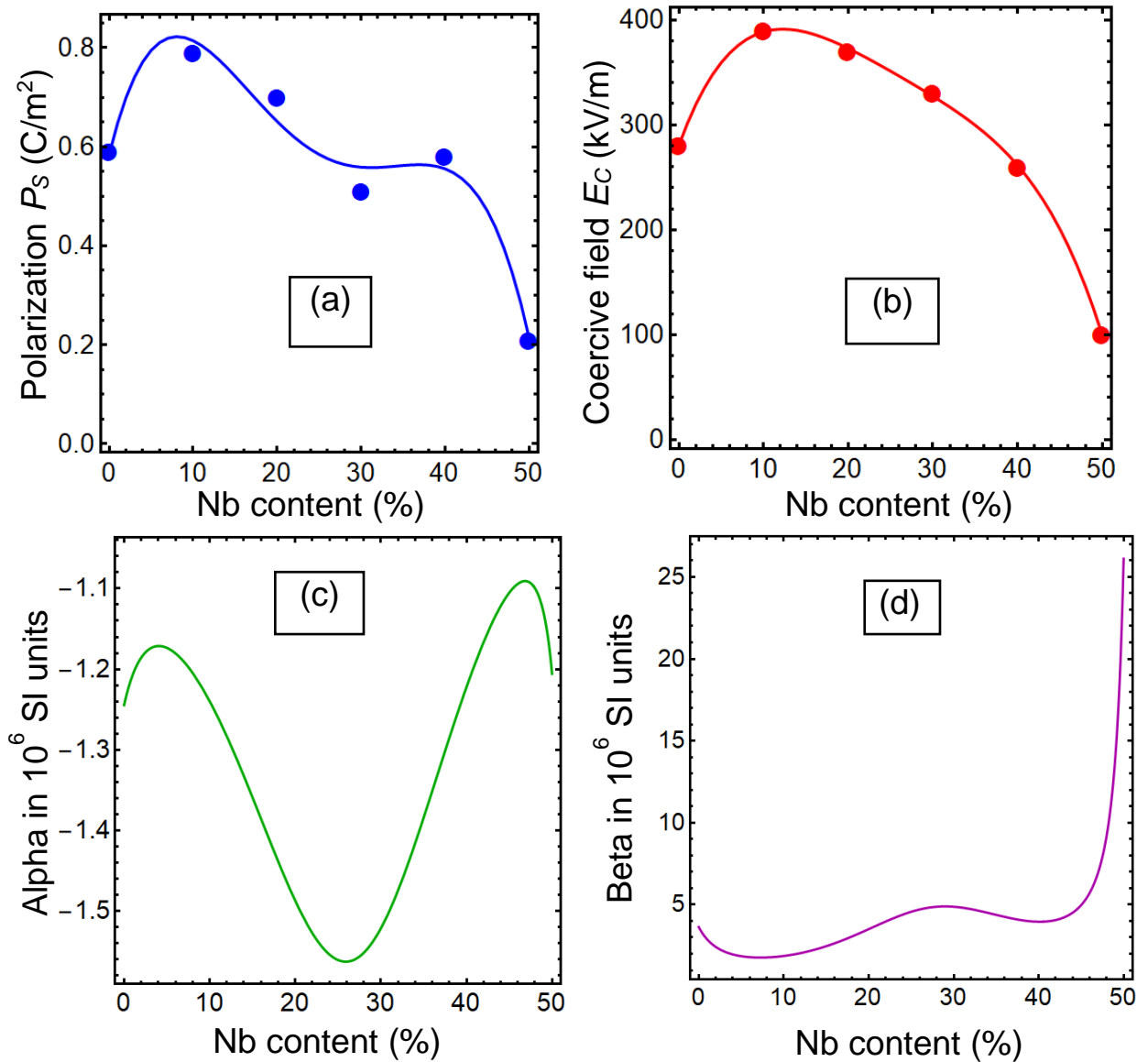


**Fig. 9.** Dependence of spontaneous polarization **(a)** of coercive field **(b)**, Landau expansion coefficients  $\alpha(T, x)$  **(c)** and  $\beta(x)$  **(d)** on Nb concentration, calculated from equations (3) for SBTN at different Nb concentrations (as a percentage) at room temperature. The symbols in graphs **(a)** and **(b)** are experimental results [33].

As follows from **Fig. 10a**, SBTN film with Nb content of 10 and 20 wt. % is as close as possible to the perovskite structure. An increase above 20 wt. % in the Nb concentration leads to a decrease in the content of the perovskite phase, as is evidenced by the expansion of the XRD line (115) and a decrease in its intensity at the angle  $2\theta \sim 28.9$  deg in **Fig. 2**. The change in the content

of the perovskite phase with the introduction of the niobium ion into the  $\text{SryBi}_{2+x}\text{Ta}_2\text{O}_9$  matrix can be explained by the change in the parameters of the crystal lattice, its bond strength and rigidity, and the surface energy of the material. The appearance of anisotropy of the crystal structure leads to a decrease in the content of the perovskite phase in the SBTN film, with an increase above 20% in the niobium impurity content. An increase to 50 wt. % in the content of niobium in the SBTN film leads to the formation of cylindrical grains with an average size of  $R = 105 \pm 3 \text{ nm}$ ,  $L = 200 \pm 3 \text{ nm}$ , which leads to the deterioration of the ferroelectric properties ( $P_s = 2.1 \mu\text{C}/\text{cm}^2$ , see **Fig. 9a**). The average grain size increases with the increase of Nb concentration above 30 wt % and it is about (100-120) nm (the crystallite size in this case is 23 nm). With the content of niobium of 50 wt %, SEM and AFM images shown in **Fig. 10b** and **10c**, demonstrate the formation of elongated quasi-ellipsoidal grains. With the decrease in the Nb concentration to 10-20 wt.%, the surface of the film has a finer grain structure (average grain size about 83-86 nm).

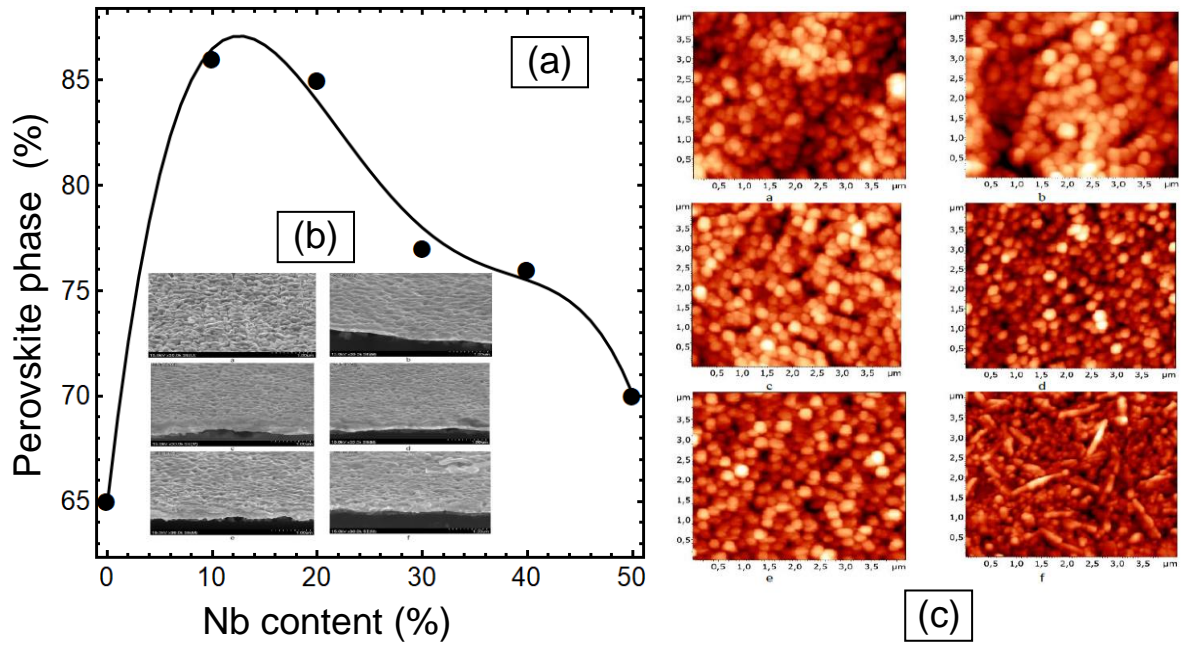


**Fig. 10.** (a) Dependence of the fraction of the perovskite phase (in percent) on the Nb concentration, calculated from equations (3a) for SBTN at different Nb concentrations (in percent). (b) SEM-images of SBT and SBTN-films: A – SBT-film, SBTN-films with Nb content: b – 10%, c – 20%, d – 30%, e – 40%, f – 50% (c) AFM-images of the SBT and SBTN-films surface: a – SBT-film, SBTN-films with content of Nb: b – 10%, c – 20%, d – 30%, e – 40%, f – 50%. Symbols, SEM and AFM images are experimental results [33].

It is reasonable to assume that  $P_S(T, x)$  is proportional to the fraction of the perovskite phase, and this is confirmed by comparing the shape of solid curves in **Fig.9a** and **Fig.10a**. This comparison is an additional basis for the applicability of equations (3) to the analysis of experimental results in order to determine the previously unknown dependences of the Landau free energy coefficients  $\alpha(T, x)$  and  $\beta(x)$  on the Nb concentration. Hence, the comparison of theoretical results with experimental measurements, shown in **Figs. 9** and **10**, reveals a linear correlation between the spontaneous polarization of nanogranular SBTNs films and the fraction of the perovskite phase in them. This is an additional basis for the applicability of the Landau approach to the analysis of experimental results in order to determine the previously unknown dependences of the Landau expansion coefficients on the concentration of dopants.

## 5. CONCLUSION

In summary, SBTN thin films doped by Nb (x=10, 20, 30, 40 and 50%) were prepared by annealing temperatures ranging from 700 to 900 °C. The relative intensity of (200) peak in XRD depended strongly on the concentration of Nb. Raman spectroscopy was successfully used to study the lattice vibrational modes and structural transition of SBT thin films with various Nb-dopant concentrations at Ta-sites. Raman spectroscopy studies can be used to study the crystallization behavior of the films. Raman spectra show that the films are polycrystalline in nature. The change of the Raman band from 810 to 830  $\text{cm}^{-1}$  is associated to the amount of Nb doped concentration and defects present in the film, which in term is related to the crystallization degree of the SBT material. The lowest Raman mode frequency near 100  $\text{cm}^{-1}$  increases with increase in Nb concentrations, whereas the octahedral stretching mode near 575  $\text{cm}^{-1}$  decreases with partial substitution of Nb for up to 30% and again increased with higher Nb contents. This behavior was explained in terms of smaller ionic radii of Nb than Ta at B-site. The lowest optical mode softened with the increase in temperature and is increased with the increase in Nb contents in SBT compounds. The substitution of Nb at Ta-site showed a significant splitting of O-Ta-O octahedral stretching mode.

Theoretical results obtained on these samples show the similarities and support Raman data. In particular, Landau approach can explain the experimentally observed fraction of perovskite phase in SBTN at annealing temperatures 800 and 900°C allowing possible appearance of finite size effects related with nanogranular structure of the studied SBTN films.

**Acknowledgements.** The work (O.M.F., A.D.Y., T.V.T., O.P.B. and A.N.M.) is supported by the National Research Foundation of Ukraine (Grant application Ф81/41481 “Cooperative kinetics of defects and domain structures in ferroelectrics”).

**Authors' contribution.** O.M.F., A.D.Y., T.V.T., O.P.B. conducted experiments and wrote the experimental part of the work. A.V.S and V.V.S. prepared samples. A.N.M. performed calculations and wrote the theoretical part of the work. All authors worked on the results discussion and manuscript improvement.

## References

1. Y. Shimakawa, Y. Kubo, Y. Nakagawa, T. Kamiyama, and H. Asano, F. Izumi. Crystal structures and ferroelectric properties of SrBi<sub>2</sub>Ta<sub>2</sub>O<sub>9</sub> and Sr<sub>0.8</sub>Bi<sub>2.2</sub>Ta<sub>2</sub>O<sub>9</sub>. *Appl. Phys. Lett.* **74**, 1904 (1999)
2. G. Senthil Murugan, and K. B. R. Varma. *Journal of Electroceramics* 8, 37-48 (2002).
3. A. Moure, and L. Pardo. *Journal of Electroceramics* 15, 243-250 (2005).
4. R. E. Jones Jr, Peter Zurcher, B. Jiang, J. Z. Witowski, Y. T. Lii, P. Chu, D. J. Taylor, and S. J. Gillespie. *Integrated Ferroelectrics* 12, 23-31 (1996).
5. J. F. Scott and C. A. Paz de Araujo, *Science* **246**, 1400 (1989).
6. C.A. Paz de Araujo, J.D. Cuchiaro, L.D. Mcmillan, M.C. Scott, J.F. Scott, *Nature* 374, 627 (1995).
7. Y. Noguchi, A. Kitamura, L.C. Woo, M. Miyayama, K. Oikawa, T. Kamiyama, *J. Appl. Phys.* 94, 6749 (2003).
8. Y. Yan, M. M. Al-Jassim, Z. Xu, X. Lu, D. Viehland, M. Payne, and S. J. Pennycook. *Applied Physics Letters* **75**, 1961-1963 (1999).
9. V.V. Sidsky, A.V. Semchenko, A.G. Rybakov, V.V. Kolos, A.S. Turtsevich, A.N. Asadchy, W. Strek. *Journal of Rare Earths.* 32, 277–281 (2014).
10. Y. Wu, M. J. Forbess, S. Seraji, Steven J. Limmer, T. P. Chou, G. Cao. *Materials Science and Engineering*, **B86**, 70–78 (2001).
11. T. C. Chen, T. Li, X. Zhang, and S. B. Desu, *J. Mater. Res.* 12, 2165 1997.
12. S. B. Desu, P. C. Joshi, X. Zhang, and S. O. Ryu, *Appl. Phys. Lett.* 71, 1041 1997.
13. T. Atsuki, N. Soyama, T. Yonezawa, and K. Ogi, *Jpn. J. Appl. Phys.*, Part 1 34, 5096 ~1995.
14. Y. Ito, M. Ushikubo, S. Yokoyama, H. Matsunaga, T. Atsuki, T. Yonezawa, and K. Ogi, *Jpn. J. Appl. Phys.*, Part 1 35, 4925 1996.
15. G. D. Hu, I. H. Wilson, J. B. Xu, W. Y. Cheung, S. P. Wong, and H. K. Wong. Structure control and characterization of SrBi<sub>2</sub>Ta<sub>2</sub>O<sub>9</sub> thin films by a modified annealing method. *Applied Physics Letters* 74, 1221 (1999); doi: 10.1063/1.123505
16. S. B. Desu and D. P. Vijay, *Mater. Sci. Eng.*, B 32, 83 1995.

---

17. E. Ching-Prado, W. Pérez, A. Reynés-Figueroa, R. S. Katiyar , D. Ravichandran & A. S. Bhalla (1999) Raman study of SrBi<sub>2</sub>Ta<sub>2</sub>O<sub>9</sub> thin films, *Ferroelectrics Letters Section*, 25:3-4, 97-102, DOI: 10.1080/07315179908204589

18. P.R. Graves, G. Hua, S. Myhra, and J.G. Thompson, *J. Solid State Chem.*, 114, 112 (1995).

19. S. Kojima, R. Imaizumi, S. Hamazaki, and M. Takashige, *Jpn. J. Appl. Phys.*, 33,5559 (1994).

20. P.R. Graves, G. Hua, S. Myhra, and J.G. Thompson, *J. Solid State Chem.*, 114, 112 (1995)

21. S. B. Desu and D. P. Vijay, *Mater. Sci. Eng.*, B 32, 83 1995.

22. Khakhomov S.A., Semchenko A.V., Sidsky V.V., Gaishun V.E., Luca D., Kolos V.V., Solodukha V.A., Pyatlitski A.N., Kovalchuk N.S. Nanostructure and ferroelectric properties of sol-gel SBTN-films for electronic devices.

23. Ortega N, Bhattacharya P and Katiyar R S 2006 *Mater. Sci. Eng. B* 130 36

24 Moret M P, Zallen R, Newnham R E, Joshi P C and Desu S B 1998 *Phys. Rev. B* 57 5715

25. Guo Zhen Liu, et al. Raman scattering study of La-doped SrBi<sub>2</sub>Nb<sub>2</sub>O<sub>9</sub> ceramics. *Journal of Physics D: Applied Physics*, 2007, 40.24: 7817.

26. T. Yu, Z. X. Shen, W. S. Toh, J. M. Xue, and J. Wang. Size effect on the ferroelectric phase transition in SrBi<sub>2</sub>Ta<sub>2</sub>O<sub>9</sub> nanoparticles *J. Appl. Phys.*, **94**, 618, (2003)

27. H. Ke, D. C. Jia, W. Wang, Y. Zhou. Ferroelectric phase transition investigated by thermal analysis and Raman scattering in SrBi<sub>2</sub>Ta<sub>2</sub>O<sub>9</sub> nanoparticles. *Solid State Phenomena* Vols. 121-123, pp 843-846(2007)

28. N.V. Morozovsky, A.V. Semchenko, V.V. Sidsky, V.V. Kolos, A.S. Turtsevich, E.A. Eliseev, and A.N. Morozovska. Effect of annealing on the charge-voltage characteristics of SrBi<sub>2</sub>(Ta,Nb)<sub>2</sub>O<sub>9</sub> films. *Physica B: Condensed Matter*, 464, Pages 1–81 (2015)

29. E.A. Eliseev, A.V .Semchenko, Y.M.Fomichov, M. D. Glinchuk, V.V.Sidsky, V.V.Kolos, Yu.M.Peskachevsky, M.V.Silbin, N.V.Morozovsky, A.N.Morozovska. Surface and finite size effects impact on the phase diagrams, polar and dielectric properties of (Sr,Bi)Ta<sub>2</sub>O<sub>9</sub> ferroelectric nanoparticles. *J. Appl. Phys.* **119**, 204104 (2016)

30. A. K. Tagantsev and G. Gerra. *J. Appl. Phys.* **100**, 051607 (2006).

31. L.D. Landau, E.M. Lifshitz, L. P. Pitaevskii. *Electrodynamics of Continuous Media*, (Second Edition, Butterworth-Heinemann, Oxford, 1984.

32. Kumar, S. N., P. Kumar, and D. K. Agrawal. Structural, dielectric and ferroelectric properties of SBN ceramics synthesized by microwave reactive sintering technique. *Ceramics International* 38, no. 6 (2012): 5243-5250.

33. V.V. Sidsky, A.V. Semchenko, V.V. Kolos, A.N. Petlitsky, V.A. Solodukha, N.S. Kovalchuk. Influence of processing conditions on the structure and ferroelectric properties of SBTN films obtained by the sol-gel method. *Problems of physics, mathematics and technology*, no. 1 (30), 2017 17-21